MULTIPLE SLIP ON MHD CASSON FLUID FLOW WITH ALIGNED MAGNETIC FIELD EFFECTS

Supported by tetfund

S. A. Agunbiade* and T. L. Oyekunle
Department of Mathematics, University of Ilorin, Kwara State, Nigeria
*****Corresponding author: agunbiade1971@gmail.com

Received: January 09, 2021 **Accepted:** April 10, 2021

Abstract: This paper is on impacts of inclined magnetic field and multiple boundary layer slip flow of convective MHD Casson fluid through an exponentially stretching porous sheet in the presence of viscous dissipation, thermal-diffusion, diffusion-thermo and thermal radiation. The non-linear boundary layer partial differential governing equations of the flow are converted using appropriate similarity transformations to non-linear coupled ordinary differential equations (ODE). The resulted momentum, heat and mass equations are solved using collocation method based on assumed Legendre polynomial. Velocity, thermal and solutal slip, inclined magnetic field, Casson fluid parameter and other physical features have been discussed and elucidated in tables and graphs. Velocity, thermal and solutal slip declined significantly the velocity, temperature and concentration distribution respectively toward the stretching sheet, while at the free stream, the effect is not noticeable.

Keywords: Casson fluid, aligned magnetic field, slip boundary conditions

Introduction

For some decades, non-Newtonian fluid flow via a stretching sheet has gained the interest of many researchers across the globe due to its applications in industry and technology. Some of the area of its applications include; cooling of metallic sheets, polymer extrusion, paper production, just to mention but few. Casson fluid is an important kind of non-Newtonian fluids, it was a model first introduced in 1995 by Casson. Casson fluid exhibits solid characteristic when yield stress is more than the shear stress, on the other hand, it behaves as fluid under a reverse trend. Examples of these kind of fluid include; paints, honey, coal in water, jelly, human blood, soup, tomato sauce, etc.

In view of these diverse applications of Casson fluid, motivated researchers such as Saravana *et al*. (2019) studied the impact of cross diffusion and aligned magnetic field on Casson fluid flow along a stretched surface of variable thickness and revealed that the thermal flow and species boundary layers are uneven for the flow over a uniform and non-uniform thickness stretched surfaces. The analysis of multiple slips and Joules dissipation on magnetic Casson fluid over a stretching surface is investigated by Gopal *et al*. (2017). They reported that slip have tendency to control the boundary layer flow. Arifin *et al*. (2017) presented the boundary layer flow and heat transfer on Casson fluid with dust particle of a stretching sheet in the presence of aligned magnetic field. It is found that a rise in aligned angle and magnetic field parameter slowed down the velocity and speed up the temperature profiles for the phases considered. The influence of aligned magnetic field on the viscous Casson fluid boundary layer flow over a stretching sheet is analyzed by Hakeem *et al*. (2016). It is noticed that the aligned angle played an important role in controlling the magnetic field strength on the Casson fluid flow region. Agunbiade and Dada (2019) examined dissipative effects of free convective chemically reacting rotatory Rivlin-Ericksen flow through a permeable vertical plate with thermal radiation. Rao *et al*. (2017) examined the steady two-dimensional MHD convective Casson fluid boundary layer flow over a permeable stretching surface in the presence of thermal radiation and chemical reaction. It is recorded that aligned angle strengthen the magnetic field and has capacity to reduce the Nusselt and Sherwood number.

The impact of multiple slips on Jeffrey fluid model for unsteady MHD viscoelastic buoyant Nanofluid in the presence of soret and radiation over a permeable stretching sheet is presented by Khan *et al*. (2019a). It is found that the boundary layers rises in the presence of multiple slips. Mabood and Shateyi (2019) analyzed numerically, the effects of multiple slip on MHD unsteady flow over a stretching sheet with soret, suction/injection and thermal radiation. They reported that an hike in Magnetic and slip parameter leads to a reduction in velocity profile while an acceleration is noticed in temperature profile. Besthapu and Haq (2019) looked into the combined effects on thermal radiation and velocity slip on MHD along free convective nonlinear stretching surface. It is observed that skin friction is a decreasing function of velocity ratio. Thermal slip and radiation effects along a convective heated stretching sheet is examined by Raza (2019) and revealed that the slip and stretching parameters played a significant role on skin friction. Kumar *et al*. (2018) studied the flow, thermal and concentration boundary layer nature of Casson and Carreau fluids over exponential stretching surface. They recorded that Carreau fluid is highly affected by the Lorentz force when equated with the Casson fluid. Salawu and Kareem (2019) investigated viscoelastic fluid with exothermic chemical reaction in the presence of heat absorption and temperature dependent viscosity. It was noticed that reaction solution can blow up if heat source reaction is not well managed. Kamran and Naseem (2019) examined effects of radiation on the flow of Nanofluids of Ag-water and Cu-water boundary layer. The results revealed that radiation has the tendency of decreasing the temperature of the fluid.

Hayat *et al*. (2016) presented cattaneo-christov heat flux model effects on heat transfer of a Jeffery fluid over a stretching surface and realized that a larger Schmidt number retard the concentration profiles. Halder *et al*. (2020) investigated the impacts of entropy in a hydromagnetic unsteady viscous fluid flow via a stretched exponentially sheet. It is noted that the velocity declined and Lorentz force became strong as the value of magnetic field increased. The effects of thermophoresis on a dissipative MHD viscous fluid flow through a stretched exponentially surface is explained by Jyothi *et al*. (2015). It was noticed that thermophoresis had a decreasing effect on concentration profile. Das *et al*. (2020) analyzed the significant of Joule heating viscous dissipation, magnetic field and slip condition on the boundary layer flow of an electrically conducting Boussinesq couple-stress fluid induced by a stretched exponentially sheet. There observation shown that the velocity profile diminished considerably within the boundary layer in the presence of a magnetic field and slip condition. The velocity and thermal slip conditions at the surface of a exponentially stretching sheet is examined by Mukhopadhyay and Gorla (2012). They recorded that the velocity and thermal slip parameters have decreasing impact on temperature. Zaib *et al*. (2019) inspected the influence of

entropy generation on aligned magnetic flow with nano particles through a convectively heated radial stretched surface in the existence of cattaneo-christov heat flux. It is observed that the velocity of nano liquid decreases while the temperature and concentration of nano liquid increase due to an aligned angle. Effects of entropy generation on MHD non-Newtonian nanofluid via a porous unsteady stretching surface is discussed by Butt *et al*. (2019) and reported that unsteadiness enhanced the generation of Entropy effects. Ali *et al*. (2019) studied the effects of multiple slip on unsteady MHD Maxwell nanofluid flow via a porous stretching sheet in the presence of thermal radiation, thermo-diffusion and chemical reaction. They concluded that an increase in the suction, slip and unsteadiness parameters slow down the velocity profiles. The effect of multiple slips on axisymmetric MHD buoyant nanofluid flow over a stretching sheet with radiation and chemical reaction are examined by khan *et al*. (2019b). It is revealed that the multiple slip effects raised the boundary layers.

In this study, efforts have been devoted to scrutinise the impacts of multiple slip on MHD Casson fluid flow through an exponential porous stretching sheet with aligned magnetic effects. This, to the best of our knowledge has not been considered in the literature. The partial differential equations governed the flow were transformed to ordinary differential equations (ODE), using appropriate similarity transformation. These equations were solved to obtain results for velocity, temperature and concentration, using collocation method with the aid of assumed Legendre polynomial and Mathematical 11.0 software.

Mathematical formulation

A laminar two dimensional steady incompressible electrically conducting Casson fluid through an exponentially stretching porous sheet with an angle of inclination δ to the vertical sheet is examined. The $x-axis$ is along the stretching sheet, which is in the direction of the flow motion, while $\eta-axis$ is taken perpendicular to it. The velocity, temperature and concentration distribution is considered to be $U=U_o e^{\frac{x}{n}}$, $\phi_w=\phi_\infty+\phi_o e^{\frac{x}{2n}}$ and $\zeta_w=\zeta_\infty+\zeta_o e^{\frac{x}{2n}}$ respectively. Since the fluid is considered to be electrically conducting, an induced magnetic field which is generated in an electrically insulator fluid due to the flow of electrical current is negligible compared to applied magnetic field. Hence, there is application of variable magnetic field $B(x)=B_o e^{\frac{x}{2n}}$ normal to the stretching sheet.

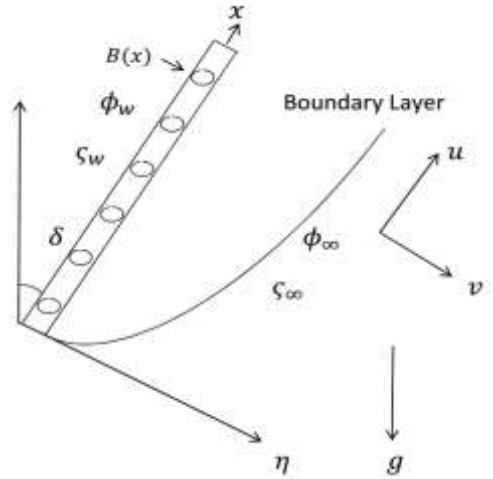

Fig. 1: Sketch of the flow model

Rheological equation of state for an incompressible isotropic Casson fluid is assumed (Reddy (2016)) as

$$\tau_{ij}=\begin{cases}2(\beta_A+\frac{T_y}{\sqrt{2\pi}})f_{ij}, \pi>\pi_d\\ 2(\beta_A+\frac{T_y}{\sqrt{2\pi}})f_{ij}, \pi<\pi_d\end{cases} \quad (1)$$

Where: β_A, T_y, $\pi=f_{ij}$, π_d, are plastic dynamic viscosity for non-Newtonian fluid, yield stress, $(ij)^{th}$ deformation rate component and product critical value for the model, respectively. This type of flow are governed by the following continuity, momentum, energy and concentration equations (Reddy *et al*., 2020);

$$\frac{\partial u}{\partial x}+\frac{\partial v}{\partial \eta}=0 \quad (2)$$

$$u\frac{\partial u}{\partial x}+v\frac{\partial u}{\partial \eta}=\nu\left(1+\frac{1}{\psi}\right)\frac{\partial^2 u}{\partial \eta^2}-\frac{\sigma B(x)^2}{\rho}(\sin\delta)^2 u+\frac{\nu}{k'}u+g\beta_\phi(\phi-\phi_\infty)+g\beta_\zeta(\zeta-\zeta_\infty) \quad (3)$$

$$u\frac{\partial \phi}{\partial x}+v\frac{\partial \phi}{\partial \eta}=\frac{k}{\rho C_p}\frac{\partial^2\phi}{\partial \eta^2}-\frac{1}{\rho C_p}\frac{\partial q_r}{\partial \eta}+\frac{\nu}{C_p}\left(1+\frac{1}{\psi}\right)\left(\frac{\partial u}{\partial \eta}\right)^2-\frac{\sigma B(x)^2}{\rho C_p}(\sin\delta)^2u^2+\frac{Q_1}{\rho C_p}(\phi-\phi_\infty)+\frac{DK_\phi}{\zeta_s C_p}\frac{\partial^2\zeta}{\partial \eta^2} \quad (4)$$

$$u\frac{\partial \zeta}{\partial x}+v\frac{\partial \zeta}{\partial \eta}=D\frac{\partial^2\zeta}{\partial \eta^2}+\frac{DK_\phi}{\phi_m}\frac{\partial^2\phi}{\partial \eta^2}-C_r(\zeta-\zeta_\infty) \quad (5)$$

with the boundary conditions

$$\left.\begin{aligned}&u=U+H\mu\frac{\partial u}{\partial \eta}, v=-V(x),\\ &\phi=\phi_w+R\frac{\partial \phi}{\partial \eta}, \zeta=\zeta_w+E\frac{\partial \zeta}{\partial \eta} at \eta=0\\ &u\to 0, \phi\to\phi_\infty, \zeta\to\zeta_\infty as \eta\to\infty\end{aligned}\right\} \quad (6)$$

Where: $H=H_1e^{-\frac{x}{2n}}$, $R=R_1e^{-\frac{x}{2n}}$ and $E=E_1e^{-\frac{x}{2n}}$; H, R, E, are the velocity, thermal and solutal slip factor respectively. By setting H, R and E to zero, no-slip conditions can be obtained. The permeability of the porous medium is $k'=k_1e^{-\frac{x}{n}}$, $C_r=k_oe^{\frac{x}{n}}$ is the reaction rate, $V(x)=V_oe^{\frac{x}{2n}}$ is the velocity at the wall, $Q_1=Q_oe^{\frac{x}{n}}$ is the heat source parameter and $\nu=\frac{\mu}{\rho}$ is the kinematic viscosity.

Method of solution

The simulation of the thermal radiation is done using Rossland approximation for diffusion, hence the radiative heat flux is expressed as

$$q_r=-\frac{4\sigma}{3k^*}\frac{\partial\phi^4}{\partial\eta} \quad (7)$$

Where: k^* is the coefficient of the mean absorption and σ is the Stefan-Boltzmann constant. With the assumption that temperature differences within the flow is sufficiently small, linearization of equation (7) can be done using Taylor's series to expand ϕ^4 and ignoring higher order terms, gives

$$\phi^4\cong 4\phi_\infty^3-3\phi_\infty^4 \quad (8)$$

With equations (7) and (8), equation (4) becomes

$$u\frac{\partial \phi}{\partial x}+v\frac{\partial \phi}{\partial \eta}=\frac{k}{\rho C_p}\frac{\partial^2\phi}{\partial \eta^2}+\frac{1}{\rho C_p}\frac{16\sigma\phi_\infty^3}{3k^*}\frac{\partial^2\phi}{\partial \eta^2}+\frac{\nu}{C_p}\left(1+\frac{1}{\psi}\right)\left(\frac{\partial u}{\partial \eta}\right)^2-\frac{\sigma B(x)^2}{\rho C_p}(\sin\delta)^2u^2+\frac{Q_1}{\rho C_p}(\phi-\phi_\infty)+\frac{DK_\phi}{\zeta_s C_p}\frac{\partial^2\zeta}{\partial \eta^2} \quad (9)$$

The following similarity variables (eqs. 10) are introduced to equations (3), (5), (6) and (9) to obtain equations (11), (12), (13) and (14)

$$\left.\begin{aligned}\xi = \left(\frac{U_o}{2\nu n}\right)^{\frac{1}{2}} e^{\frac{x}{2n}}\eta, U = U_o e^{\frac{x}{n}} f'(\xi), v = -\sqrt{\frac{\nu U_o}{2n}}\, e^{\frac{x}{2n}} f(\xi)\\ \phi = \phi_\infty + \phi_o e^{\frac{x}{2n}}\vartheta(\xi), \zeta = \zeta_\infty + \zeta_o e^{\frac{x}{2n}}\varphi(\xi)\end{aligned}\right\} \quad (10)$$

$$\left(1+\frac{1}{\psi}\right) f''' - 2(f')^2 + ff'' - (M\sin^2\delta + K)f' + \lambda_1\vartheta + \lambda_2\varphi = 0 \quad (11)$$

$$\frac{1}{P_r}\left(1+\frac{4}{3}N\right)\vartheta'' + f\vartheta' - f'\vartheta + E_c\left(1+\frac{1}{\psi}\right)(f'')^2 + M\sin^2\delta E_c(f')^2 + Q\vartheta + D_p\varphi'' = 0 \quad (12)$$

$$\varphi'' + S_c f\varphi' - S_c f'\varphi - S_c k_r\varphi + S_c S_p\vartheta'' = 0 \quad (13)$$

The associated boundary conditions are

$$\left.\begin{aligned}f(\xi) = S,\ f'(\xi) = 1 + S_1 f''(\xi),\ \vartheta(\xi) = 1 + S_2\vartheta'(\xi),\ \varphi(\xi) = 1 + S_3\varphi'(\xi)\ at\ \xi = 0\\ f'(\xi) \to 0,\ \vartheta(\xi) \to 0,\ \varphi(\xi) \to 0\ as\ \xi \to \infty\end{aligned}\right\} (14)$$

where $M = \frac{2\sigma B_o^2 n}{\rho U_o}$ is magnetic parameter, $S_p = \frac{DK_\phi\phi_o}{\phi_m\zeta_o\nu}$ is Soret number, $P_r = \frac{\rho\nu C_p}{k}$ is the Prandtl number, $N = \frac{4\sigma\phi_\infty^3}{k^* k}$ is the radiation parameter, $E_c = \frac{U_o^2}{C_p\phi_o} e^{\frac{3x}{2n}}$ is Eckert number, $S = \frac{V_o}{\sqrt{\frac{U_o\nu}{2n}}}$ is suction, $K = \frac{2\nu n}{k_1 U_o}$ is permeability parameter, $k_r = \frac{2nk_o}{U_o}$ is the chemical recation, $Q = \frac{2nQ_o}{\rho C_p U_o}$ is the heat source, $S_c = \frac{\nu}{D}$ is the Schmidth number, $D_p = \frac{DK_\phi\zeta_o}{\zeta_s C_p \nu\phi_o}$ is Dufour number, $G_h = \frac{2g\beta_\phi(\phi_w - \phi_\infty)nx^2}{\nu^2}$ is the Grashof number, $Re_x = \frac{xU_o e^{\frac{x}{n}}}{\nu}$ is the local Reynolds number, $\lambda_1 = \frac{G_h}{Re_x^2}$ is buoyancy parameter, $G_m = \frac{2g\beta_\zeta(\zeta_w - \zeta_\infty)nx^2}{\nu^2}$ is the solutal Grashof number, $\lambda_2 = \frac{G_m}{Re_x^2}$ is the solutal buoyancy parameter, $S_1 = H_1\rho\sqrt{\frac{\nu U_o}{2n}}$ is the velocity slip, $S_2 = R_1\sqrt{\frac{U_o}{2\nu n}}$ is the thermal slip and $S_3 = E_1\sqrt{\frac{U_o}{2\nu n}}$ is the solutal slip.

Equations (11), (12) and (13) with the boundary conditions (14) are obtained using collocation method with the aid of assumed Legendre polynomial. Given the assumed Legendre polynomial

$$f = \sum_{j=0}^{W} a_j(\eta)P_j \quad (15)$$

The transformation $\eta = \frac{2\xi}{L} - 1$ is used to transform the Legendre polynomial from $[-1,1]$ to $[0,L]$. Hence,

$$f = \sum_{j=0}^{W} a_j(\eta)P_j \Rightarrow f(\xi) = \sum_{j=0}^{W} a_j\left(\frac{2\xi}{L} - 1\right)P_j(\xi) j = 0,1,2,3,4,\ldots,W \quad (16)$$

The boundary value problem interval of $[0,\infty)$ is transformed to $[0,L]$ using the domain truncation method. Therefore, Eqs. (11), (12) and (13) are solved within the region $[0,L]$ instead of $[0,\infty)$. Velocity, temperature and concentration distributions solutions are obtained using MATHEMATICA 11.0 software. For this problem, the physical quantities of interest; coefficient of skin-friction, rate of heat and mass transfer are defined below;

$$C_f = \frac{2\beta_w}{\rho U_o^2 e^{\frac{2x}{n}}}, Nu_x = \frac{x\gamma_w}{k(\phi_w - \phi_\infty)} and Sh_x = \frac{x\Omega_w}{D(\zeta_w - \zeta_\infty)} \quad (17)$$

where β_w, γ_w,Ω_w are shear stress, heat flux and mass flux of the surface respectively given as

$$\beta_w = \mu\left(\frac{\partial u}{\partial\eta}\right)_{\eta=0}, \gamma_w = -k\left(\frac{\partial\phi}{\partial\eta}\right)_{\eta=0}, and\Omega_w = -D\left(\frac{\partial\zeta}{\partial\eta}\right)_{\eta=0}, \quad (18)$$

Substituting equations (10) and (18) to (17) gives

$$\frac{C_f\sqrt{\frac{Re_x}{2}}}{\sqrt{\frac{x}{n}}} = f''(0), \frac{Nu_x}{\sqrt{\frac{Re_x}{2}}\sqrt{\frac{x}{n}}} = -\vartheta'(0) and \frac{Sh_x}{\sqrt{\frac{Re_x}{2}}\sqrt{\frac{x}{n}}} = -\varphi'(0) \quad (19)$$

Results and Discussion

The non-linear coupled ODEs (11), (12) and (13) along with the boundary conditions (14) are solved using Collocation method with the aid of assumed Legendre polynomial. The computation is carried out for different pertinent parameters; Eckert number E_c, Angle of Inclination δ, Casson parameter ψ, Radiation parameter N, Prandtl number P_r, Chemical reaction parameter k_r, Suction parameter S, Velocity slip S_1, Thermal slip S_2, Solutal slip S_3, Dufour number D_p, Soret number S_p, buoyancy parameter λ_1, Solutal buoyancy parameter λ_2, Permeability parameter K, Schmidth number S_c, Magnetic parameter M and Heat source parameter Q. The default values used are; $E_c = S_2 = S_3 = D_p = Q = 0.1$, $\psi = N = S = S_1 = 0.5$, $P_r = 0.71$, $\delta = \frac{\pi}{4}$, $k_r = M = 1.0$, $\lambda_1 = \lambda_2 = K = 2.0$, $S_p = 0.8$ and $S_c = 0.6$. The comparison in this work is done using Runge-Kutta method as shown in Table 6 and the result of Collocation method is found to be in excellent agreement with Runge-Kutta 4th Order method.

Figures 2 and 3 depict the variation of the inclination angle (δ) with temperature and velocity distribution, respectively. It is found that a rise in δ enhanced the temperature profile as presented in Fig. 2 and diminished the velocity profile as shown in Fig. 3. Actually, the impact of larger values of δ is to build a stronger impression on the external magnetic field.

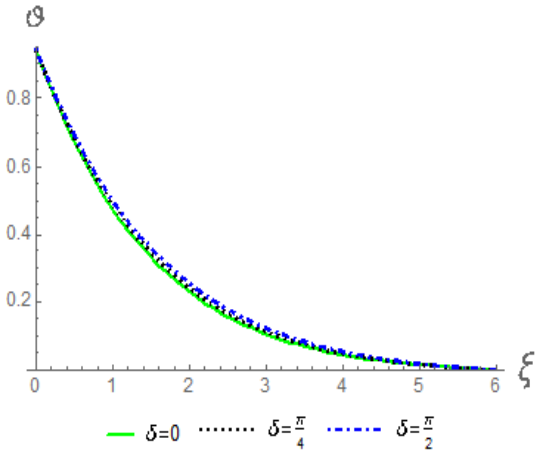

Fig. 2: Temperature with δ

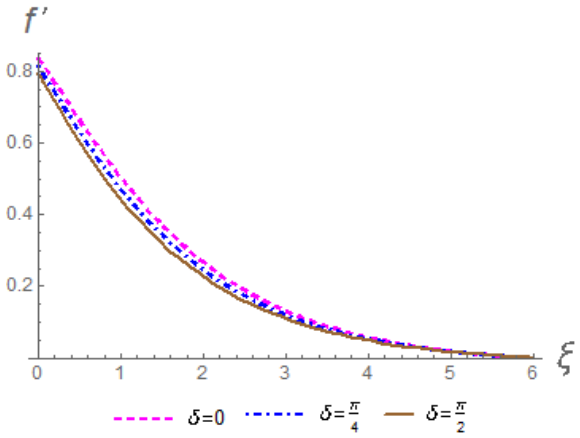

Fig. 3: Velocity with δ

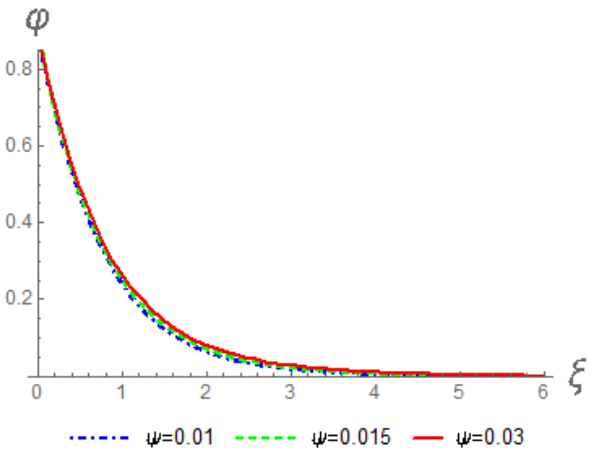

Fig. 4: Concentration with ψ

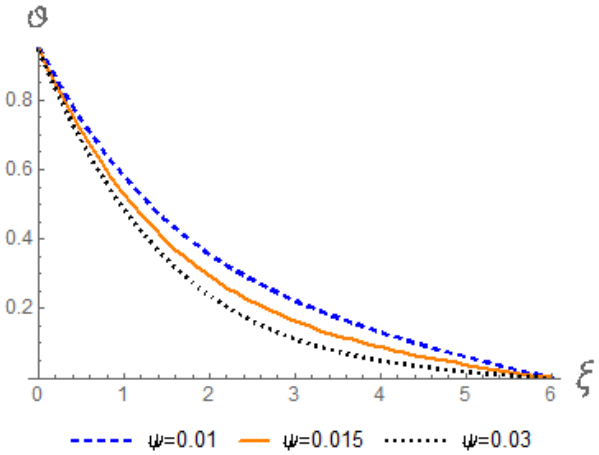

Fig. 5: Temperature with ψ

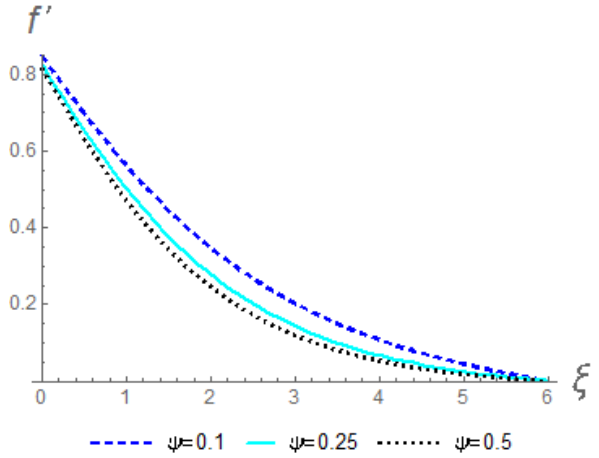

Fig. 6: Velocity with ψ

The influence of Casson parameter ψ on concentration, temperature and velocity profiles is highlighted in Figs. 4, 5 and 6, respectively. It is noticed that an increase in ψ gives rise to concentration profile as shown in Fig. 4 and reduces the temperature and velocity profiles as presented in Figs. 5 and 6, respectively. Physically, fluid begins to behave like a rigid body for bigger value of ψ since the viscosity of the fluid is also higher at which there is high tendency of flow velocity to decrease.

Figures 7, 8 and 9 scrutinize the impact of solutal slip (S_3), thermal slip (S_2) and velocity slip (S_1) on concentration, temperature and velocity profiles respectively. An increase in S_3, S_2 and S_1 leads to a decrease in concentration and temperature profiles while a decrease up to $\xi = 1.9$ is noticed before a slight increase is realized in velocity profile. In reality, the fluid becomes more viscous and resulted to reduction in the fluid flow and momentum boundary layer thickness whenever there is a rise in slip parameter.

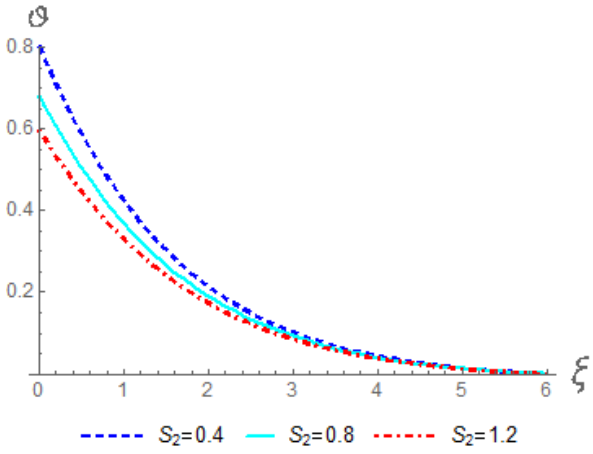

Fig. 7: Concentration with S_3

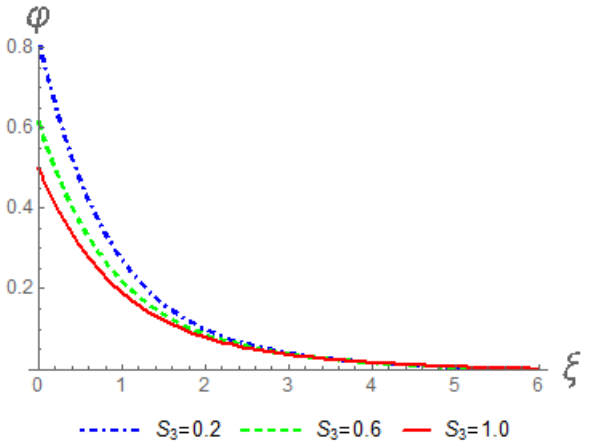

Fig. 8: Temperature with S_2

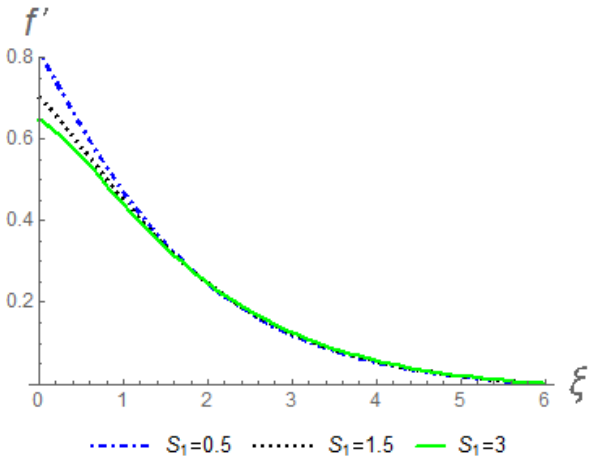

Fig. 9: Velocity with S_1

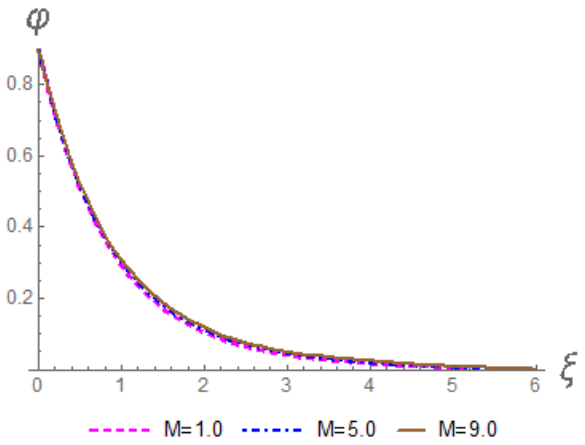

Fig. 10: Concentration with *M*

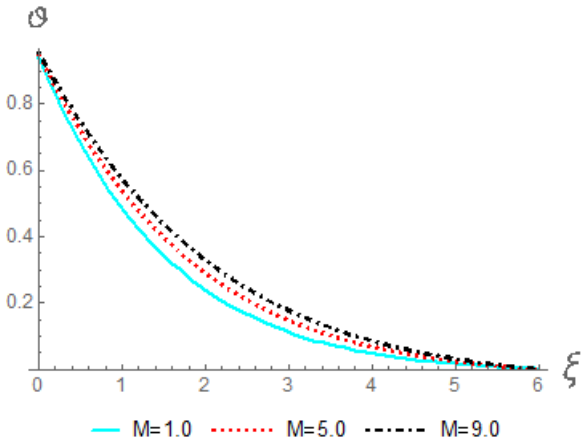

Fig. 11: Temperature with *M*

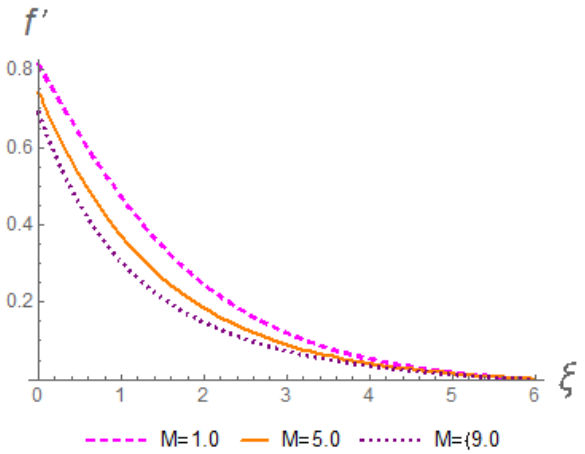

Fig. 12: Velocity with *M*

Figures 10, 11 and 12 portray the effect of magnetic field parameter (M) on concentration, temperature and velocity distribution. The concentration and temperature distribution are enhanced while a retardation in velocity distribution is observed with an increase in the M as shown respectively in the Figures. The development of M is enhanced with an increase in angle of inclination (δ) which in turns generate the Lorentz force that act opposite to the flow direction and slower the mobility of the fluid flow.

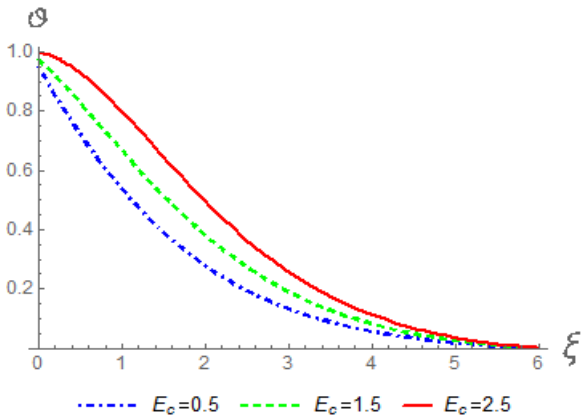

Fig. 13: Temperature with E_c

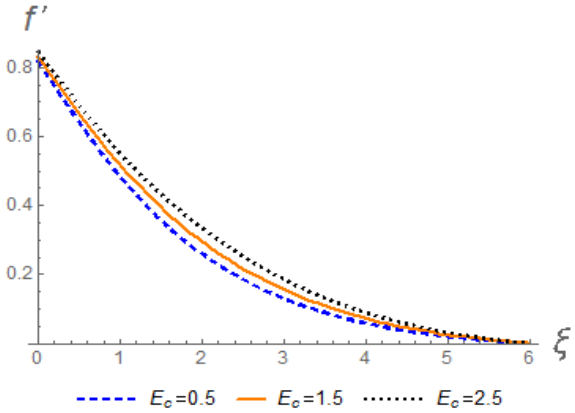

Fig. 14: Velocity with E_c

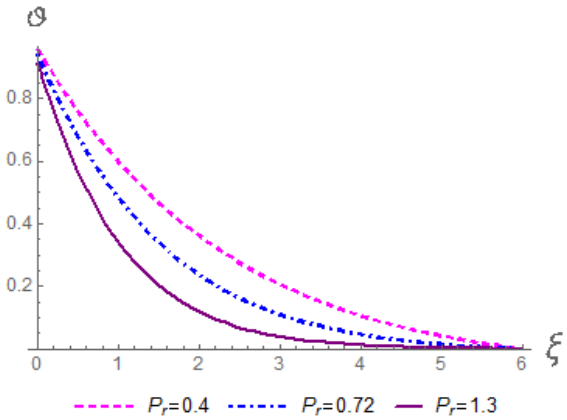

Fig. 15: Temperature with P_r

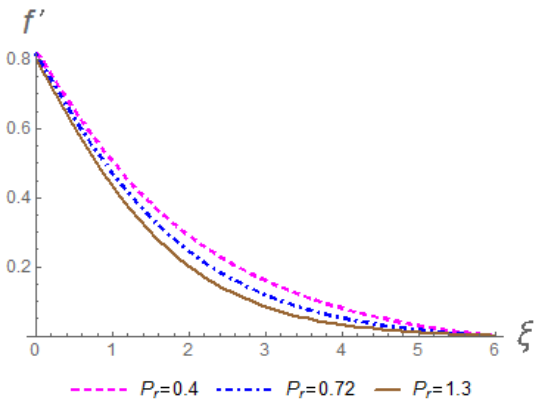

Fig. 16: Velocity with P_r

The impact of Eckert number (E_c) on temperature and velocity profiles is established in Figs. 13 and 14. It is discovered that both the temperature and velocity accelerate with an increase in E_c. This is as a result of reduction in the surface rate of heat transfer for higher values of E_c. Eventually, temperature of the fluid increases because of internal molecular friction that convert mechanical energy to heat energy. Reverse in their behaviour is the case with a rise in Prandtl number (P_r) as registered in Figs. 15 and 16, respectively. Physically, larger P_r is to lower thermal diffusivity and thus weaken the thermal boundary layer thickness.

Figures 17 and 18 show the effect of soret (S_p) and Dufour (D_p) parameters on the concentration and temperature profiles respectively. It is seen that the concentration increase with an hike in S_p. The same trend is noticed with a rise in D_p on temperature profile. Impact of radiation parameter (N) is displayed in Figure 19. It is worthy to note that, radiation energises the flow and enhances the fluid heat. Hence, thermal boundary layer thickness improves for higher values of N.

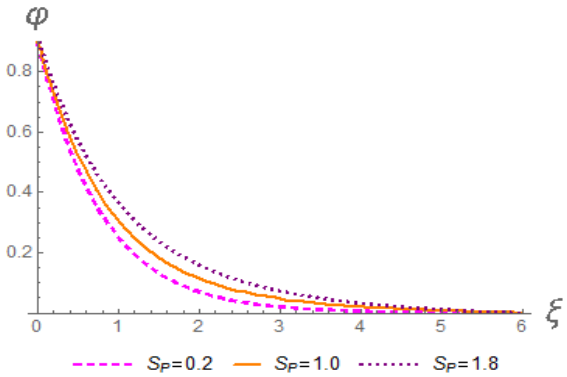

Fig. 17: Concentration with S_p

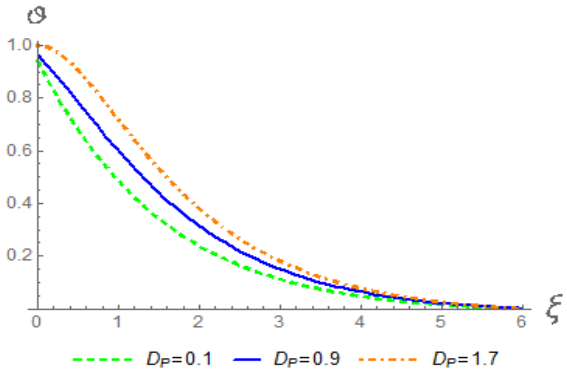

Fig. 18: Temperature with D_p

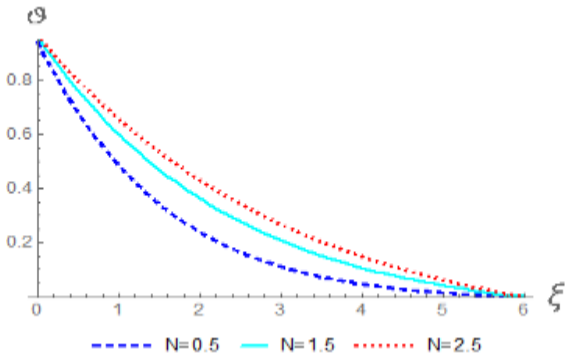

Fig. 19: Temperature with N

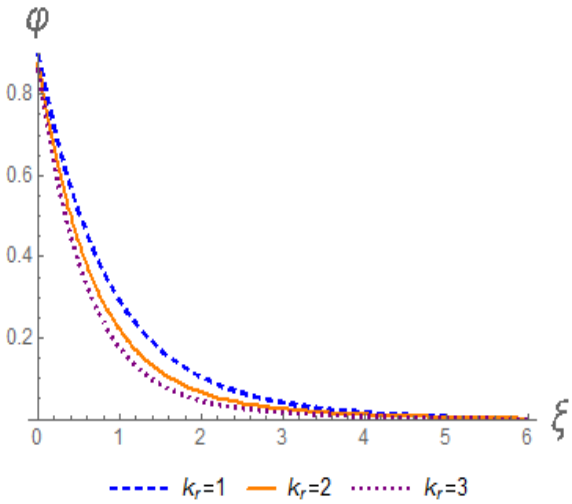

Fig. 20: Concentration with k_r

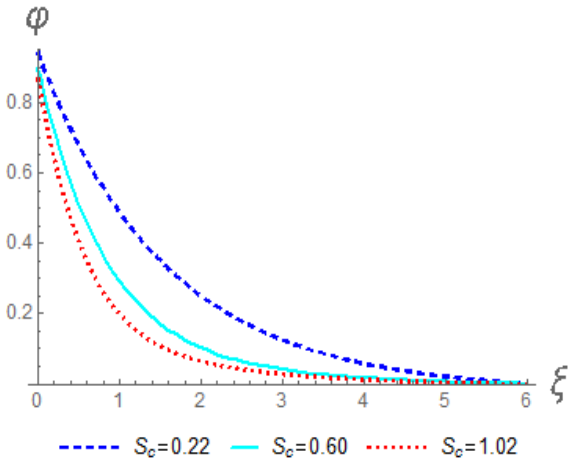

Fig. 21: Concentration with S_c

Figures 20 and 21 depict the variation of chemical reaction (k_r) and Schmidth (S_c) parameters on the concentration profile. It is realized that concentration decelerated in the boundary layer with increase in k_r, this resulted from the fact that the thickness of the solutal boundary layer is declined due to destructive chemical which in turn improve the mass transfer. S_c leads to a depression in concentration profile. Physically, a push in S_c give a reverse in molecular diffusion.

Table 1: Values of Skin-friction, Nusselt number and Sherwood Number for different values of D_p, S_p, λ_1, λ_2, K,S_c and M

D_p	S_p	λ_1	λ_2	K	S_c	M	$-f''(0)$	$-\vartheta''(0)$	$-\varphi''(0)$
0.1	0.8	2.0	2.0	2.0	0.6	1.0	0.37076	1.01604	0.59975
0.7	0.8	2.0	2.0	2.0	0.6	1.0	0.35452	1.08718	0.40712
0.1	1.3	2.0	2.0	2.0	0.6	1.0	0.36311	0.94598	0.60732
0.1	0.8	3.0	2.0	2.0	0.6	1.0	0.28282	1.02926	0.63108
0.1	0.8	2.0	3.0	2.0	0.6	1.0	0.30182	1.02586	0.62065
0.1	0.8	2.0	2.0	3.0	0.6	1.0	0.44798	1.00453	0.56836
0.1	0.8	2.0	2.0	2.0	1.02	1.0	0.39367	1.33605	0.57650
0.1	0.8	2.0	2.0	2.0	0.6	1.5	0.39096	1.01446	0.58735

Table 2: Values of Skin-friction, Nusselt number and Sherwood Number for different values of E_c, δ, ψ, N, P_r, k_r,S and Q

E_c	δ	ψ	N	P_r	k_r	S	Q	$-f''(0)$	$-\vartheta'(0)$	$-\varphi'(0)$
0.1	$\frac{\pi}{4}$	0.5	0.5	0.71	1.0	0.5	0.1	0.37076	1.01604	0.59975
0.6	$\frac{\pi}{4}$	0.5	0.5	0.71	1.0	0.5	0.1	0.35871	1.05989	0.47720
0.1	$\frac{\pi}{3}$	0.5	0.5	0.71	1.0	0.5	0.1	0.39096	1.01446	0.58735
0.1	$\frac{\pi}{4}$	0.9	0.5	0.71	1.0	0.5	0.1	0.38207	1.01214	0.59635
0.1	$\frac{\pi}{4}$	0.5	1.0	0.71	1.0	0.5	0.1	0.35704	1.05095	0.49576
0.1	$\frac{\pi}{4}$	0.5	0.5	1.0	1.0	0.5	0.1	0.38604	0.96925	0.73307
0.1	$\frac{\pi}{4}$	0.5	0.5	0.71	3.0	0.5	0.1	0.39909	1.39715	0.57055
0.1	$\frac{\pi}{4}$	0.5	0.5	0.71	1.0	0.9	0.1	0.41100	1.09049	0.68272
0.1	$\frac{\pi}{4}$	0.5	0.5	0.71	1.0	0.5	0.6	0.47252	0.91629	0.90543

Table 3: Velocity slip effect on Skin-friction, Heat transfer and Mass transfer coefficient

S_1	$-f''(0)$	$-\vartheta'(0)$	$-\varphi'(0)$
0.5	0.37076	1.01604	0.59975
0.9	0.27519	1.00601	0.58996
1.2	0.23077	1.00137	0.58505

Table 4: Thermal slip effect on Skin-friction, Heat transfer and Mass transfer coefficient

S_2	$-f''(0)$	$-\vartheta'(0)$	$-\varphi'(0)$
0.1	0.37076	1.01604	0.59975
0.4	0.39896	1.03081	0.49235
0.7	0.41909	1.04065	0.41869

Table 5: Solutal slip effect on Skin-friction, Heat transfer and Mass transfer coefficient

S_3	$-f''(0)$	$-\vartheta'(0)$	$-\varphi'(0)$
0.1	0.37076	1.01604	0.59975
0.4	0.40052	0.75529	0.59906
0.7	0.41839	0.60184	0.59845

Table 6: Comparison of Collocation and Runge-Kutta 4th order method for Skin-friction

D_p	S_p	N	ψ	E_c	M	Collocation method	R-K 4th Order
0.1	0.8	0.5	0.5	0.1	1.0	0.37076	0.37076
0.5	0.8	0.5	0.5	0.1	1.0	0.35999	0.35999
0.1	1.0	0.5	0.5	0.1	1.0	0.36772	0.36772
0.1	0.8	0.8	0.5	0.1	1.0	0.36180	0.36180
0.1	0.8	0.5	0.8	0.1	1.0	0.38024	0.38024
0.1	0.8	0.5	0.5	0.4	1.0	0.36352	0.36352
0.1	0.8	0.5	0.5	0.1	2.0	0.41035	0.41035

The impact of various physical parameters on skin friction, heat transfer and mass transfer coefficient is displayed in Tables 1 and 2. Table 3, 4 and 5 portray velocity, thermal and solutal slip influence on skin friction, heat transfer and mass transfer coefficient, respectively. Table 3 shows that skin friction, heat transfer and mass transfer coefficient decelerate with a rise in S_1. It is evident in Table 4 that both skin friction and heat transfer coefficient is enhanced while mass transfer coefficient dropped with a hike in S_2. Table 5 reveals that S_3 has the tendency of enhancing skin friction and declining both heat transfer and mass transfer coefficient.

Conclusion

In this study, an analysis of multiple slip on MHD Casson fluid flow through an exponentially porous stretching sheet with aligned magnetic field effects is carried out. The partial differential equations governed the fluid flow are transformed to ordinary differential equations by applying suitable similarity transformation. These equations were solved numerically, using collocation method based on assumed Legendre polynomial. The effects of various embedded parameters on fluid physical properties were examined and illustrated in graphs and tables. The following conclusions are drawn from the study;

(i) The velocity profile depreciated with an increase in δ, ψ, M, P_r and appreciated with S_1 and E_c.

(ii) The temperature profile declines due to ψ, S_2, P_r and improved with δ, M, E_c, D_p and N.

(iii) The concentration profiles is depressed due to S_3, k_r,S_c and elevated with ψ, M and S_p.

Slip conditions which is more appropriate in non-Newtonian fluids such as Casson fluid is applicable in melting of many polymers which exhibit wall slip as a result of relationship between the velocity slip and traction. In various industrial processes, there can arise the slip effects at the boundaries of walls, pipes, etc. Hence, this study has its applications in coating and suspensions, metallic plate cooling, and in processing of materials.

Nomenclature

u and v components of velocity along x and η directions, respectively (ms^{-1})
g acceleration as a result of gravity (m/s^2)
C_p Specific heat at constant pressure ($Jkg^{-1}K^{-1}$)
k thermal conductivity
q_r radiative heat flux
D species diffusivity
K_ϕ thermal diffusion ratio
U_o reference velocity
n reference length

Greek symbols

μ dynamic viscosity
ρ density of the fluid (kgm^{-3})
ψ Casson parameter
σ electrical conductivity (W/m^2k^4)
ξ similarity variable
ϑ dimensionless temperature
φ dimensionless concentration
ϕ_o reference temperature
ζ_o reference concentration
β_ϕ coefficient of thermal expansion ($m^3/kmol$)
β_ζ coefficient of solutal expansion (K^{-1})
ϕ the fluid temperature (K)
ϕ_∞ far away temperature from the sheet
ζ the fluid concentration ($kmol/m^3$)
ζ_∞ far away concentration from the sheet ($kmol/m^3$)
ζ_s concentration susceptibility
ϕ_m mean fluid temperature
δ Inclination angle from the vertical direction

Conflict of Interest

The authors declare that there is no conflict of interest related to this study.

References

Agunbiade SA & Dada MS 2019. Effects of viscous dissipation on convective rotatory chemically reacting Rivlin-Ericksen flow past a porous vertical plate. *J. Taibah Univ. for Sci.*, 13(1): 402-413. DOI: 10.1080/16583655.2019.1582149

Ali B, Nie Y, Khan SA, Sadiq MT & Tariq M 2019. Finite element simulation of multiple slip effects on MHD unsteady Maxwell nanofluid flow over a permeable stretching sheet with radiation. *Processes*, 7(9): 1-18.

Arifin NS, Zokri SM, Kasim AM, Salleh MZ, Yusoff WNS, Mohammad NF & Shafie S 2017. Aligned magnetic field on dusty Casson fluid over a stretching sheet with Newtonian heating. *Malaysian J. Fundam. and Appl. Sci.*, 3(3): 244-247.

Besthapu P, Haq RU, Bandari S & Al-Mdallal QM 2019. Thermal radiation and slip effects on MHD stagnation point flow of non-Newtonian nanofluid over a convective stretching surface. *Neural Comput. Appl.*, 31(1): 207-217.

Butt AS, Ali A, Nazimtufail M & Shafie S 2019. Theoretical investigation of entropy generation effects in magnetohydrodynamic flow of Casson Nanofluid over an unsteady permeable stretching surface. *J. Nanofluids*, 8(1): 103-116.

Das S, Patra RR & Jana RN 2020. The layout of Boussinesq couple-stress fluid flow over an exponentially stretching sheet with slip in porous space subject to a variable field. *Multidiscipline Modeling in Materials and Structures*, https://doi.org/10.1108/mmm-09-2019-0168

Gopal D, Kishan N & Raju CSK 2017. Viscous and joule's dissipation on Casson fluid over a chemically reacting stretching sheet with inclined magnetic field and multiple *slips Informatics in Medicine Unlocked*, 9: 154-160.

Halder S, Bult AS, Li Y, Imran SM, Ahmad B & Tayyaba A 2020. Study of entropy generation with multi-slip effects in MHD unsteady flow of viscous fluid past an exponentially stretching surface. *Symmetry*, 12(426) doi:10.3390/sym12030426

Hakeem AA, Renuka P, Ganesh NV, Kalaivanan R & Ganga B 2016. Influence of inclined Lorentz forces on boundary layer flow of Casson fluid over an impermeable stretching sheet with heat transfer. *Journal of Magnetism and Magnetic Materials*, **(**401): 354-361.

Hayat T, Khan MI, Alsaedi A, Waqas M & Yasmeen T 2016. Impact of cattaneo-christov heat flux model in flow of variable thermal conductivity fluid over a variable thick surface. *Int. J. Heat and Mass Transfer*, 99: 702-710.

Jyothi KP, Sreelakshmi K & Nagendramma VS 2015. Study of thermophpresis on the MHD flow due to an exponentially stretching sheet in the presence of viscous dissipation. *Proc. Eng.*, 127: 340-346.

Kamran A & Naseem A 2019. Radiation effects on boundary layer flow of Cu-water and An-water Nanofluids over a stretching plate with suction and heat transfer with convective surface boundary condition. *Applic. and Appl. Maths: An Int. J.* (AAM), 14(1): 312-321.

Khan SA, Nie Y & Ali B 2019a. Multiple slip effects on MHD unsteady viscoelastic nano-fluid flow over a permeable stretching sheet with radiation using the finite element method. *S N Applied Sci.*, (2): 66. https://doi/10-1007/542452-019-183

Khan SA, Nie Y & Ali B 2019b. Multiple slip effects on MHD axisymmetric buoyant nanofluid flow above a stretching sheet with radiation and chemical reaction. *Symmetry*, 11(9): 1-18. https://doi.org/10.3390/sym11091171

Kumar MS, Sandeep N, Kumar BR & Dinesh PA 2018. A comparative analysis of MHD non-Newtonian flow over an exponential stretched sheet. *Alexandria Engineering Journal*, 57(3): 2093-2100.

Mabood F & Shateyi S 2019. Multiple slip effect on MHD unsteady flow heat and mass transfer impinging on permeable stretching sheet with radiation. *Modelling and Simulation in Engineering*, 1-11, https://doi.org/10.1155/2019/3052790

Mukhopadhyay S & Gorla RSR 2012. Effects of partial slip on boundary layer flow past a permeable exponential stretching sheet in the presence of thermal radiation. *Heat Mass Tranf.*, 48(10): 1773-1781.

Rao ME & Sreenadh S 2017. MHD flow of a Casson fluid over an exponentially inclined permeable stretching surface with thermal radiation, viscous dissipation and chemical reaction. *Global J. Pure and Appl. Maths.*, 13(13): 7529-7548.

Raza J 2019. Thermal radiation and slip effects on MHD stagnation point flow of Casson fluid over a convective stretching sheet. *Propulsion and Power Research*, 8(2): 138-146.

Reddy BN, Maddileti P & Reddy BS 2020. Combined impact of viscous dissipation, heat source and radiation on MHD flow past an exponentially stretching sheet with Soret and Dufour effects. *Int. J. Innov. Techn. and Exploring Engr.*, 9(4): 342-347. DOI:10.35940/ijitee.D1188.029420

Reddy PBA 2016. Magnetohydrodynamic flow of a Casson fluid over an exponentially inclined permeable stretching surface with thermal radiation and chemical reaction. *Aim Shams Engineering Journal*, 1-9. http://dx.doi.org/10.1016/j.asej.2015.12.010

Salawu SO & Kareem RA 2019. Analysis of heat absorption viscoelastic exothermic chemical reaction fluid with temperature dependent viscosity under bimolecular kinetic. *Applic. and Appl. Maths: An Int. J.* (AAM), 14(2): 1232-1242.

Saravana R, Sailaja M & Reddy RH 2019. Effect of aligned magnetic field on Casson fluid flow over a stretched surface on non-uniform thickness. *Nonlinear Engineering*, 8(1): 283-292.

Zaib A, Khan U, Khan I, Selkh AH & Sherif EM 2019. Numerical investigation of aligned magnetic flow comprising nano liquid over a radial stretchable surface with cattaneo-christov heat flux with entropy generation. *Symmetry*, 11(12): 1-19. https://doi.org/10.3390/sym11121520